Urea and Urea Nitrate Decomposition Pathways: A Quantum Chemistry Study

Igor V. Tokmakov,[†] Saman Alavi,[‡] and Donald L. Thompson*,[†]

Department of Chemistry, University of Missouri−Columbia, Columbia, Missouri 65211, and Steacie Institute for Molecular Sciences, National Research Council of Canada, 100 Sussex Drive, Ottawa, Ontario K1A 0R6, Canada

Received: November 8, 2005; In Final Form: January 11, 2006

Electronic structure calculations have been performed to investigate the initial steps in the gas-phase decomposition of urea and urea nitrate. The most favorable decomposition pathway for an isolated urea molecule leads to HNCO and NH_3. Gaseous urea nitrate formed by the association of urea and HNO_3 has two isomeric forms, both of which are acid−base complexes stabilized by the hydrogen-bonding interactions involving the acidic proton of HNO_3 and either the O or N atoms of urea, with binding energies ($D_0°$, calculated at the G2M level with BSSE correction) of 13.7 and 8.3 kcal/mol, respectively, and with estimated standard enthalpies of formation ($\Delta_f H_{298}°$) of −102.3 and −97.1 kcal/mol, respectively. Both isomers can undergo relatively facile double proton transfer within cyclic hydrogen-bonded structures. In both cases, HNO_3 plays a catalytic role for the (1,3) H-shifts in urea by acting as a donor of the first and an acceptor of the second protons transferred in a relay fashion. The double proton transfer in the carbonyl/hydrogen bond complex mediates the keto−enol tautomerization of urea, and in the other complex the result is the breakdown of the urea part to the HNCO and NH_3 fragments. The enolic form of urea is not expected to accumulate in significant quantities due to its very fast conversion back to $H_2NC(O)NH_2$ which is barrierless in the presence of HNO_3. The HNO_3-catalyzed breakdown of urea to HNCO and NH_3 is predicted to be the most favorable decomposition pathway for gaseous urea nitrate. Thus, HNCO + NH_3 + HNO_3 and their association products (e.g., ammonium nitrate and isocyanate) are expected to be the major initial products of the urea nitrate decomposition. This prediction is consistent with the experimental *T*-jump/FTIR data [Hiyoshi et al. *12th Int. Detonation Symp.*, Aug 11−16, San Diego, CA, 2002].

I. Introduction

Salts composed of an organic cation and an oxygen-rich anion comprise an important class of energetic materials with the attractive property that fuel and oxidizer components can be combined in a single stable compound. By varying the chemical nature of either or both ions, an energetic material can be tailored to fit specific requirements. Consideration of environmental impact and toxicity is particularly important in the design of energetic materials. Thus, organic nitrates and dinitramides (salts of $HN(NO_2)_2$), which are typically biodegradable and produce environmentally relatively benign combustion products, are of prime interest as replacements for conventional inorganic energetic salts such as ammonium perchlorate.

We report here the results of an electronic structure study of the mechanisms and energetics of the gas-phase decomposition of urea and urea nitrate. Urea nitrate (UN) is a relatively stable and well-studied representative of energetic organic salts. The practical use of UN as an explosive is limited due to its strong acidity. Nevertheless, UN is a relatively low-cost, low-sensitivity, and high-performance energetic material suitable for experimental and modeling studies of general detonation phenomena. Its detonation properties have been studied experimentally[1−3] and computationally.[4]

Two principal decomposition channels have been suggested for UN(s) (we distinguish solid-phase urea nitrate UN(s) from an isolated UN(g) molecule) based on a *T*-jump/FTIR spectroscopic study:[5]

$$UN(s) \rightarrow (NH_3 + HNO_3) + HNCO \quad (1)$$

$$UN(s) \rightarrow NH_3 + N_2O + CO_2 + H_2O \quad (2)$$

Channel (1) accounts for the formation of HNCO observed in the early stages of pyrolysis and for the appearance of ammonium nitrate (NH_4NO_3) vapor at longer reaction times. However, if the reaction occurs under harsher conditions, CO_2 and N_2O are produced in higher concentrations than HNCO, presumably by a different channel (2). In addition, NH_3, H_2O, ammonium isocyanate (NH_4NCO), and small amounts of NO and NO_2 have been identified among the products of the UN(s) pyrolysis. Nitric acid was also observed but only for a very short time (3−5 s) in the beginning of the decomposition reaction, probably from the reversible UN dissociation to urea, $NH_2C(O)NH_2$, and HNO_3:[5]

$$UN(s) \rightleftharpoons UN(g) \quad (3)$$

$$UN(g) \rightleftharpoons HNO_3 + NH_2C(O)NH_2 \quad (4)$$

Interestingly, gaseous urea could not be detected at the same conditions. Its disappearance was explained by a fast rearrangement to NH_4NCO. However, the mechanistic details of this reaction as well as the elementary steps involved in the decomposition channels (1) and (2) could not be unambiguously determined from the spectroscopic data.

[†] University of Missouri−Columbia.
[‡] National Research Council of Canada.
* Corresponding author. E-mail: thompsondon@missouri.edu.

10.1021/jp0564647 CCC: $33.50
Published on Web 02/08/2006

SCHEME 1

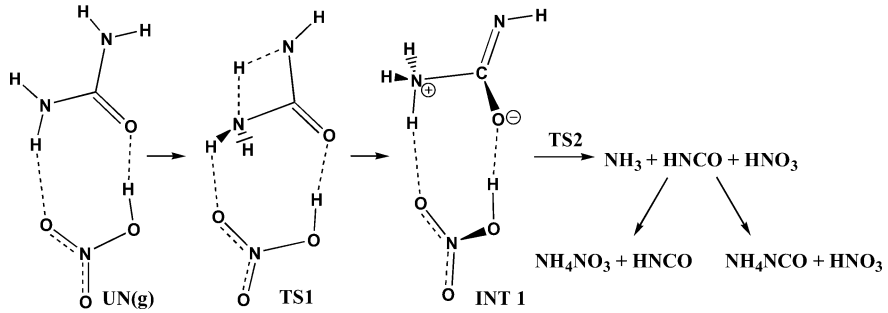

SCHEME 2

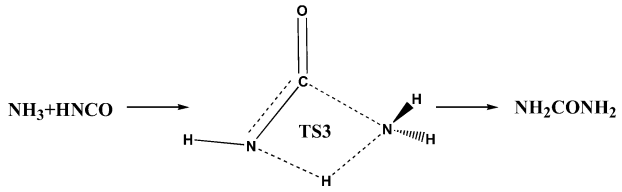

A decomposition pathway for UN(g) was proposed by Kohno et al.[6] on the basis of quantum-chemical calculations at the HF, B3LYP, and MP2 levels of theory with the 6-31++G(2d,p) basis set. They found that the isolated UN molecule has the structure of an eight-membered cyclic acid−base complex $[(NH_2)_2CO\cdots HONO_2]$ stabilized by two hydrogen bonds and calculated the potential energy profile for the two-step decomposition sequence (Scheme 1). The first step is (1,3) H-transfer between the two NH_2 groups of urea. Then NH_3 is eliminated from the zwitterionic intermediate formed in the first step. Finally, NH_3 can react with HNCO and HNO_3 to produce the experimentally observed ammonium isocyanate (NH_4NCO) and nitrate (NH_4NO_3), respectively.[5] There is a barrier of 48 kcal/mol (MP2/6-31++G(2d,p), $T = 0$ K) for the urea part to decompose into NH_3 and HNCO fragments. This barrier is much higher than the dissociation energy of UN(g) to urea and nitric acid calculated at the same level of theory which is $\Delta_{(4)}H_0^\circ = 14.0$ kcal/mol, implying that detectable amounts of gaseous urea and HNO_3 should have been produced in the early stages of the UN pyrolysis.[5] As mentioned above, gaseous urea was not observed in the *T*-jump/FTIR pyrolytic study[5] of urea nitrate, suggesting that an alternative, more facile process must be responsible for the rapid conversion of urea to HNCO and NH_3 in the presence of nitric acid.

The reverse reaction of urea synthesis from NH_3 and HNCO (or NH_4NCO) is the Wöhler reaction[7] which occurs spontaneously in water solution and in solid NH_4NCO open to the atmosphere. Recently, the mechanism of this reaction was investigated by Tsipis and Karipidis[8,9] using quantum-chemical calculations at the B3LYP/6-31G(d,p) and CBS-QB3 levels of theory and by Estiu and Merz[10] at the solvent-corrected MP2/6-311++G(d,p) level. The gas-phase bimolecular reaction of NH_3 with HNCO to form urea proceeds via a four-center transition state for the NH_3 addition to the C═N double bond in HNCO (Scheme 2). The calculated barriers (CBS-QB3, $T = 0$ K) are 33 and 49 kcal/mol for urea formation and decomposition, respectively.[9] These barriers are too high to allow a rapid conversion between NH_3 + HNCO and urea at normal conditions; however, the theoretical results[8−10] predict a significant catalytic effect of H_2O and/or NH_3 molecules on this process. The $(H_2O)_n$ or $(NH_3)_m$ catalyst molecules (cases $n = 1$, 2 and $m = 1$ were explicitly studied) facilitate the Wöhler reaction through a H-transfer relay mechanism, which involves a nucleophilic attack of NH_3 on the C atom of HNCO concerted with a series of H-shifts from the NH_3 reactant molecule to the N atom of HNCO via a hydrogen-bonded network of $(H_2O)_n$ or $(NH_3)_m$ catalyst molecules. Scheme 3 illustrates the mechanism of urea synthesis from NH_3 and HNCO catalyzed by one H_2O molecule via a six-center transition state.

This H_2O-catalyzed reaction proceeds in three steps: (1) reactants associate in a termolecular complex **R3**; (2) NH_3 adds to the C═N double bond in HNCO via a six-center transition state TS3(cat) where the H_2O molecule mediates the H-transfer in a relay fashion; (3) the H_2O and urea molecules are released from the complex **P3** produced in the previous step. The effective barrier for the H_2O-catalyzed urea synthesis (the energy of TS3(cat) relative to NH_3 + HNCO + H_2O) reported by Tsipis and Karipidis[9] is 10 kcal/mol (CBS-QB3, $T = 0$ K), which is 23 kcal/mol lower than the barrier for the uncatalyzed reaction. A qualitatively similar catalytic effect of water has been reported by Estiu and Merz[10] at the MP2/6-311++G(d,p) level of theory. The water molecule facilitates the reverse reaction as well. Thus, previous studies[8−10] suggest that at high temperature an equilibrium is expected between the reactants and products in Scheme 3 that shifts more toward NH_3 + HNCO + H_2O with increasing temperature.

The experimental study of the UN pyrolysis[5] indicates that a rapid conversion of urea to NH_3 and HNCO occurs in the early stages of the pyrolysis in the presence of nitric acid. In view of a very sizable catalytic effect of water on urea decomposition,[8−10] we envisage that nitric acid should serve as a catalyst of this process, rather than play a spectator role (cf. Scheme 1), which prompts us to look for alternative lower energy pathways for UN(g) decomposition.

II. Theoretical Methods

Quantum-chemical calculations were performed with the GAUSSIAN03 suite of programs.[11] Geometric optimization of the structures and harmonic vibrational frequency calculations were done with DFT[12,13] using the B3LYP hybrid gradient-corrected approach of Becke[14] and the recently proposed BB1K density functional.[15] The latter is a hybrid version of the BB95 density functional that mixes Becke's 1988 gradient corrected exchange[14b] and 1995 kinetic-energy-dependent correlation[16] functionals with the fraction of HF exchange optimized for the prediction of thermochemical kinetics against a data set of reaction energies and forward and reverse barriers.[15] Our choice of the B3LYP density functional is primarily due to its well-documented good performance for geometry optimization of equilibrium structures, where the B3LYP geometric parameters are typically of the same quality as those obtained at higher levels of theory, such as MP2 and QCISD.[17] The BB1K density functional, on the other hand, has been shown to provide good quality molecular and transition state geometries[15] as well as good results for a combination of thermochemical kinetics and

SCHEME 3

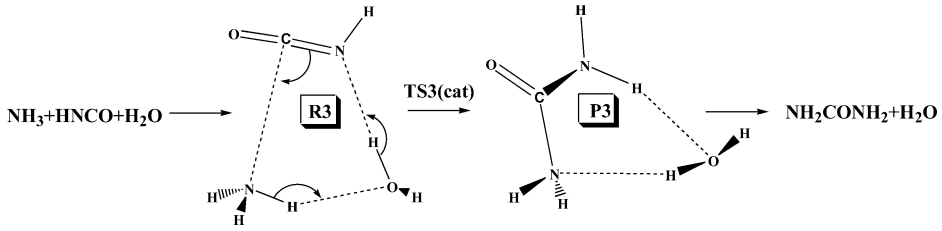

nonbonded interactions.[18,19] All geometry optimizations employed a diffuse 6-311++G(d,p) basis set[20] to better describe the long-range hydrogen bonding in the complexes of nitric acid and the transient structures with ionic character.

The decomposition mechanisms studied here involve proton transfer. Since DFT calculations are known to underestimate proton-transfer barriers in the prototypical $[H_2O^+H\cdots OH_2]$[21,22] and $[H_3N^+H\cdots NH_3]$[23] complexes, more accurate estimations were obtained with MP2 and higher level calculations. To test the accuracy of the DFT-optimized structures, we also performed some geometry optimizations at the MP2 level with the same 6-311++G(d,p) basis set. No geometric constraints were applied during the optimization calculations, which were done using the analytical gradient-based Berny[24] and modified GDIIS[25] algorithms. All stationary points were characterized by the number of imaginary vibrational frequencies. Transition states were assigned to elementary reactions in accordance with the minimum-energy paths (MEPs) calculated by following intrinsic reaction coordinates (IRC)[26] from the transition states to the reactants and products.

Previous studies[27−29] indicate that both B3LYP-DFT and MP2 methods provide accurate molecular parameters and adequate description of hydrogen-bonding and proton-transfer mechanisms in small ammonium and hydroxylammonium nitrate clusters. However, higher levels of theory must be employed to obtain more reliable energetics. Herein, higher-level energetic parameters were determined for the most important transformations by the G2M method.[30] The G2M family of composite methods is based on performing high-level single-point energy calculations on structures optimized at the B3LYP-DFT level. A number of variations of the G2M method are available, suitable for systems of different size. For the present molecules containing up to eight non-hydrogen atoms, the G2M(RCC,MP2) scheme has been chosen in this study:

$$E[\text{G2M(RCC,MP2)}] = E[\text{CCSD(T)/6-311G(d,p)}] + \Delta E(+3\text{df,2p}) + \text{ZPE} \quad \text{(I)}$$

$$\Delta E(+3\text{df,2p}) = E[\text{MP2/6-311 + G(3df,2p)}] - E[\text{MP2/6-311G(d,p)}] \quad \text{(II)}$$

This scheme approximates the CCSD(T)/6-311+G(3df,2p) electronic energy from the base energy, E[CCSD(T)/6-311G(d,p)], and a basis set extension correction, $\Delta E(+3\text{df,2p})$. The base energy is determined by the closed-shell coupled cluster singles and doubles theory augmented with a perturbation correction for triple excitations[31−35] with the standard triple-ζ basis set. The $\Delta E(+3\text{df,2p})$ term evaluated at the MP2 level of theory corrects for the absence of the diffuse and higher polarization functions in the basis set used in the calculation of the base energy. A frozen core approximation is used in the CCSD(T) and MP2 calculations.

In the present use of the G2M method, all higher-level single-point calculations were performed on the geometries optimized by the B3LYP/6-311++G(d,p) method; zero-point vibrational energy (ZPE) corrections were calculated from the unscaled vibrational frequencies obtained at the same level; and the empirical higher level corrections[30] (HLCs) were omitted. All reactions considered in this study are isogyric (have a conserved number of electron pairs in the reactants, transition states, and products), in which case HLCs cancel out in all relative energies.

III. Results and Discussion

Urea Decomposition. To better understand the decomposition mechanism of urea nitrate, we begin by briefly revisiting the transformations of an isolated urea molecule. Urea (**1**) has been the subject of a number of theoretical electronic structure studies.[36−43] Its unimolecular transformations received less attention, but the mechanisms of the two key reactions have recently been studied by Tsipis and Karipidis[8,9] at the B3LYP/6-31G(d,p) and CBS-QB3 levels of theory and by Estiu and Merz[10] at the MP2/6-311++G(d,p) level. Those two reactions are keto−enol tautomerization (eq 5) and deamination (eq 6):

$$NH_2CONH_2\ (\mathbf{1}) \xrightarrow{TS_{1-2}} NH_2C(OH)NH\ (\mathbf{2}) \quad (5)$$

$$NH_2CONH_2\ (\mathbf{1}) \xrightarrow{TS_{1-3}} NH_3 + NHCO\ (\mathbf{3}) \quad (6)$$

Other possible urea decomposition pathways, such as N−H or C−N bond scissions or H_2 elimination, are not expected to be competitive. We have investigated the most important unimolecular transformations of urea (reactions 5 and 6) using the present methods (section II). In addition, we have also considered various decomposition pathways originating from the enolic form of urea (**2**):

$$NH_2C(OH)NH\ (\mathbf{2}) \xrightarrow{TS_{2-3}} NH_3 + HNCO\ (\mathbf{3}) \quad (7)$$

$$NH_2C(OH)NH\ (\mathbf{2}) \xrightarrow{TS_{2-4}} NH_3 + HOCN\ (\mathbf{4}) \quad (8)$$

$$NH_2C(OH)NH\ (\mathbf{2}) \xrightarrow{TS_{2-5}} H_2O + HNCNH\ (\mathbf{5}) \quad (9)$$

$$NH_2C(OH)NH\ (\mathbf{2}) \xrightarrow{TS_{2-6}} H_2O + H_2NCN\ (\mathbf{6}) \quad (10)$$

The urea isomer (**2**) has four conformations (**2a**−**2d**) corresponding to different combinations of the OH torsional angle and cis−trans orientation of the imino-(N−H) bond (see Figure 1). Since each conformation is nonplanar, it exists in two enantiomeric forms. Molecular structures of conformations **2a**−**2d** and interconversion pathways between them have been computed earlier by Tsipis and Karipidis[8] at the B3LYP/6-31G(d,p) level of theory. Similar results are obtained in this work using higher level methods. Therefore, only a brief account of the energetics calculated at the highest level of theory will be given here. Further details can be found in the Supporting Information for the present and earlier[8] studies.

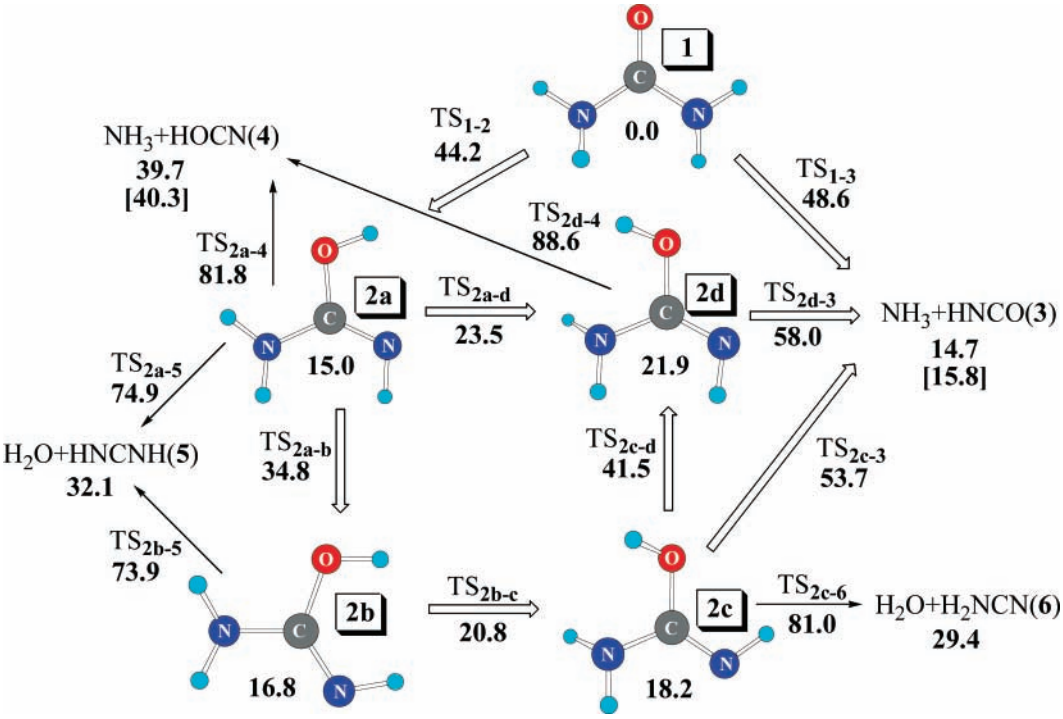

Figure 1. Urea isomerization, deamination, and dehydration pathways. All energies ($T = 0$ K, ZPE-corrected, in kcal/mol) are given relative to urea (**1**) as calculated by the G2M method; the reference values are given in square brackets.

Conformation **2a** is the lowest energy enolic form of urea. At the G2M level conformations **2b**, **2c**, and **2d** are predicted to be less stable by 1.8, 3.2, and 6.9 kcal/mol, respectively. Transitions from **2a** to **2b** and from **2d** to **2c** involve an internal rotation of the imino-(N−H) bond about the C═N double bond hindered by ∼20 kcal/mol in both cases. The torsional motion of the O−H group about the C−O bond in **2** is more facile. It connects conformations **2a** to **2d** and **2b** to **2c** over the barriers of 8.5 kcal/mol (TS_{2a-d}) and 4.0 kcal/mol (TS_{2b-c}).

Figure 1 shows the complete network of urea isomerization/decomposition pathways satisfying reactions 5−10. The most important transformations are designated by wide arrows. The energetic parameters given in Figure 1 were calculated by the G2M method, and they are used in the following discussion. Urea (**1**) may either isomerize to its tautomeric form **2a** over a barrier of 44.2 kcal/mol or eliminate the NH_3 molecule after clearing a slightly higher barrier of 48.6 kcal/mol. Our G2M estimates of these barriers are in excellent agreement with the CBS-QB3 values (44.0 and 48.6 kcal/mol) reported by Tsipis and Karipidis.[9] Four conformations of **2** may interconvert between each other and access various decomposition pathways: H_2O eliminations yielding carbodiimide HNCNH (from **2a** and **2b**) or cyanamide NH_2CN (from **2c**); NH_3 eliminations leading to either isocyanic acid HNCO (from **2c** and **2d**) or cyanic acid HOCN (from **2a** and **2d**). Among the latter processes, the NH_3 eliminations to produce HNCO via TS_{2c-3} and TS_{2d-3} have the lowest barriers. However, none of the deamination and dehydration pathways originating from the enolic forms of urea (**2a**−**2d**) are more favorable than their isomerization back to urea followed by its decomposition to NH_3 and HNCO via TS_{1-3}.

Detailed molecular structures of the species and transition states shown in Figure 1 as well as the energetics calculated at various levels of theory are provided in the Supporting Information. The predicted thermochemistry of several product channels can be benchmarked against that derived from the literature values of the enthalpies of formation ($\Delta_f H_0°$) of urea (−52.7 kcal/mol),[44] NH_3 (−9.3 ± 0.1 kcal/mol),[45] HNCO (−27.6 ± 0.2 kcal/mol),[46] and HOCN (−3.1 ± 0.2 kcal/mol).[46] The G2M energies of the NH_3 + HNCO (**3**) and NH_3 + HOCN (**4**) products relative to urea (**1**) are in good agreement (within 1.1 kcal/mol) with the reference values (see Figure 1). The energetic parameters calculated by DFT methods are less accurate. For instance, the enthalpy of urea decomposition to HNCO and NH_3 is underestimated by 3.0 kcal/mol at the B3LYP/6-311++G-(d,p) level and overestimated by 2.0 kcal/mol by the BB1K density functional with the same basis set.

Molecular Structure of Urea Nitrate. The crystal structure of urea nitrate has been determined by neutron[47] and X-ray diffraction.[48] According to these experimental studies, crystalline urea nitrate is a salt composed of the nitrate and protonated urea ions with an acidic proton attached to the O atom of urea. The molecular structure of urea nitrate in the gas phase has been studied theoretically by Kohno et al.[6] at the HF, B3LYP-DFT, and MP2 levels with the 6-31++G(2df,p) basis set. These calculations revealed that an isolated UN molecule does not exist as an ionic pair but has the structure of an acid−base molecular complex stabilized by partial donation of the acidic proton from HNO_3 to the carbonyl group of urea. However, the isomerism of the gas-phase urea nitrate has not been studied. In the present work, we explored various possibilities for the association of urea with nitric acid in the gas phase and found additional isomeric forms of the molecular complex thus produced. The corresponding structures and conformational transitions calculated by B3LYP-DFT and MP2 methods with the 6-311++G(d,p) basis set are illustrated in Figures 2 and 3, which also display the geometric parameters for the two major isomers optimized with BB1K-DFT.

The lowest energy isomer **7a** is an eight-membered cyclic acid−base complex stabilized by two hydrogen bonds. The stronger $O_{(2)}-H_{(a)}\cdots O_{(1)}$ hydrogen bond with $r(H_{(a)}\cdots O_{(1)}) \sim 1.6$ Å is between the urea O atom and the hydroxyl group of HNO_3, whereas the weaker $N_{(1)}-H_{(b)}\cdots O_{(3)}$ hydrogen bond with $r(H_{(b)}\cdots O_{(3)}) \sim 2.0$ Å links one of the urea NH_2 groups to the

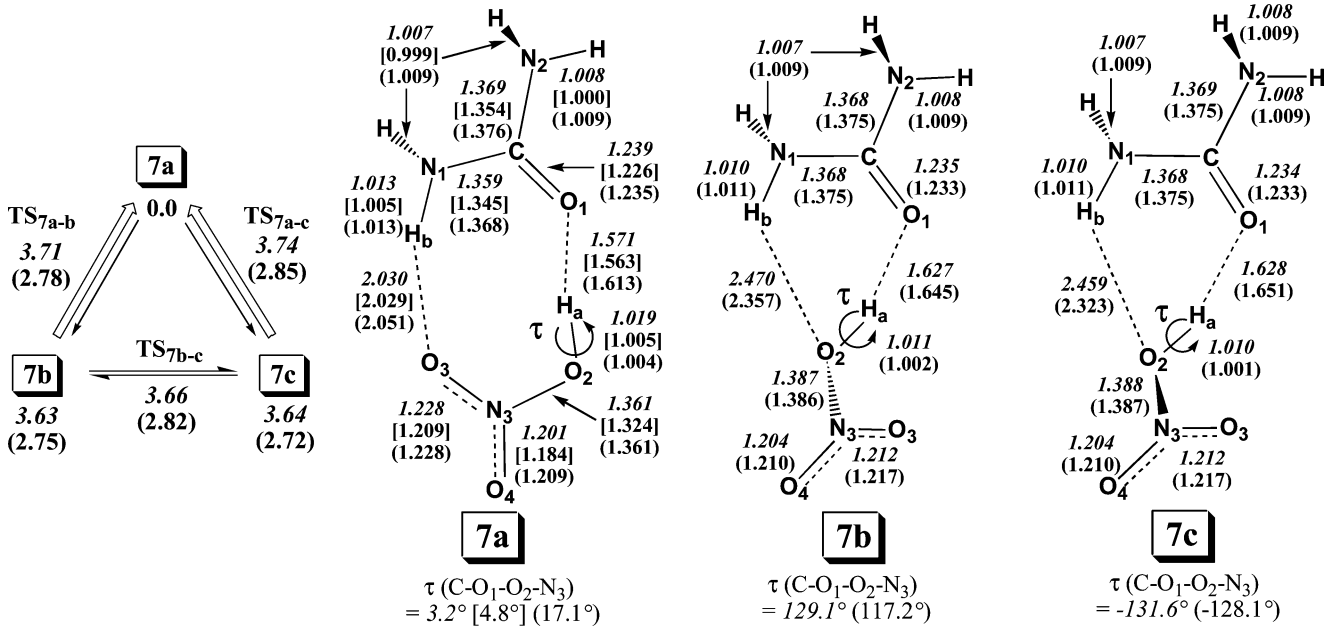

Figure 2. Interconversion scheme and molecular structures (bond lengths in Å) of the urea nitrate conformations **7a**−**7c**. Energies ($T = 0$ K, ZPE-corrected, in kcal/mol) are given relative to the most stable form **7a**. Geometric and energetic parameters were calculated using the B3LYP-DFT (values in italics), BB1K-DFT (values in square brackets), and MP2 (values in parentheses) optimization methods with the 6-311++G(d,p) basis set.

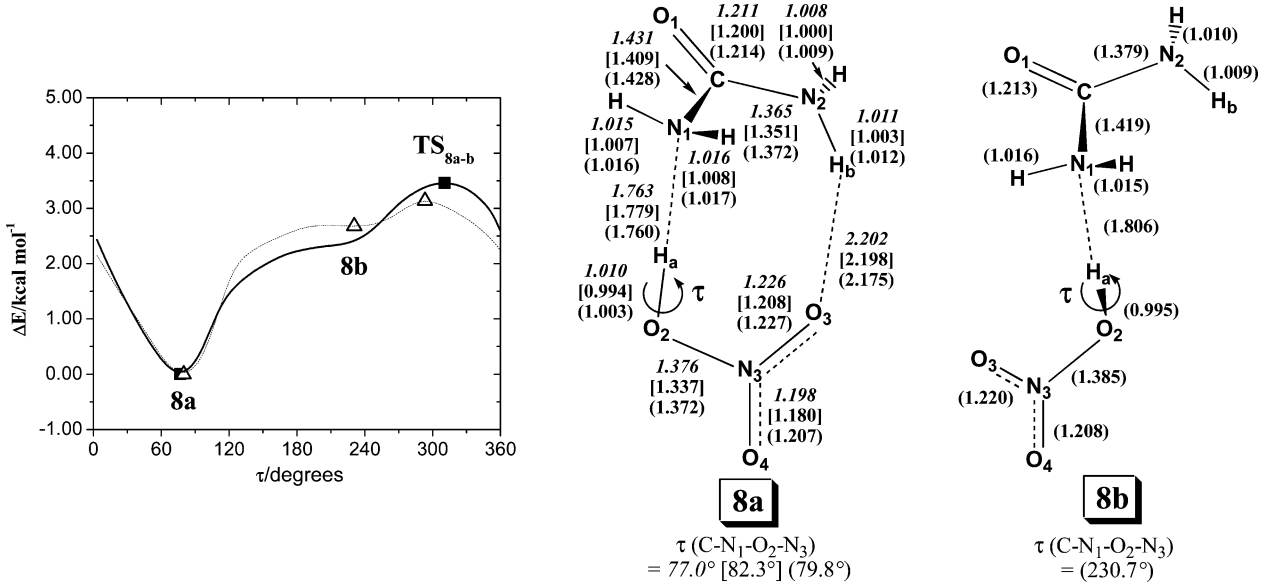

Figure 3. $N_{(3)}-O_{(2)}-H_{(a)}\cdots N_{(1)}$ torsional potential ($T = 0$ K, ZPE-correction not included) and molecular structures (bond lengths in Å) of the urea nitrate conformations **8a** and **8b**. Geometries and energies along the torsional profile were calculated using the B3LYP-DFT (solid line, values in italics), BB1K-DFT (values in square brackets), and MP2 (dashed line, values in parentheses) optimization methods with the 6-311++G(d,p) basis set.

NO_2 residue of HNO_3. By analyzing the potential energy profile for internal rotation of HNO_3 about the $O_{(2)}-H_{(a)}\cdots O_{(1)}$ bond, we found two additional nearly degenerate local minima, **7b** and **7c**. They are the six-membered hydrogen-bonded complexes with a $N_{(2)}-H_{(b)}\cdots O_{(2)}-H_{(a)}\cdots O_{(1)}$ hydrogen-bonding pattern involving the hydroxyl group of HNO_3 in a dual role of the proton donor (to the carbonyl group of urea) and acceptor (from the NH_2 group of urea). Both forms **7b** and **7c** are very shallow minima separated from each other by a torsional barrier of ≤0.1 kcal/mol. The conversion of forms **7b** and **7c** to **7a** also has a low torsional barrier of ≤0.1 kcal/mol. Besides the carbonyl group, each NH_2 group may also be a proton acceptor due to the presence of a lone electron pair on the N atom. Therefore, we have also searched for possible isomeric forms of urea nitrate stabilized by the $O_{(2)}-H_{(a)}\cdots N_{(1)}$ hydrogen bond between the hydroxyl group of HNO_3 and the N atom of urea. The complete torsion potentials for internal rotation of HNO_3 about the $O_{(2)}-H_{(a)}\cdots N_{(1)}$ bond are shown in Figure 3. Both MP2 and DFT optimization methods locate the minimum (**8a**) at $\tau \sim 80°$. This conformation allows for the second hydrogen bond to be formed between the second NH_2 group of urea and the NO_2 residue of HNO_3. Thus, in addition to the stronger $O_{(2)}-H_{(a)}\cdots N_{(1)}$ hydrogen bond with $r(H_{(a)}\cdots N_{(1)}) \sim 1.8$ Å, conformation **8a** is also stabilized by the weaker $N_{(2)}-H_{(b)}\cdots O_{(3)}$ hydrogen bond with $r(H_{(b)}\cdots O_{(3)}) \sim 2.2$ Å. The MP2-optimized torsion potential shown in Figure 3 has another minimum (**8b**) at $\tau \sim 230°$, which appears as a very small dip on the wide shoulder between form **8a** and the torsional barrier TS_{8a-b}. This small dip is not present

TABLE 1: Binding Energies[a] for the Molecular Complexes of Urea, Ammonia, and Hydroxylamine with HNO_3

	$D_0°$(**7**)		$D_0°$(**8**)		$D_0°$(AN)		$D_0°$(HAN)
method[b]	no CP	CP	no CP	CP	no CP	CP	no CP
B3LYP/6-311++G(d,p)	14.95	14.17	8.46	7.38	12.39	11.24	12.73[c]
BB1K/6-311++G(d,p)	15.39	14.52	8.81	7.66	12.54	11.40	12.89
MP2/6-311++G(d,p)	13.81	10.89	10.16	7.00	12.27	9.49	12.70[c]
MP2/6-311G(d,p)	14.88	10.47	12.14	7.37	14.25	9.18	14.61
CCSD(T)/6-311G(d,p))	15.07	10.60	12.10	7.28	13.87	8.82	14.27
MP2/6-311+G(3df,2p)	15.21	13.53	9.90	8.36	11.74	10.52	13.23
G2M(CC,MP2)	15.41	13.66	9.86	8.27	11.36	10.17	12.90

[a] ZPE-corrected, in kcal/mol, $T = 0$ K. [b] Geometry optimization was performed at the B3LYP, BB1K, and MP2 levels with the 6-311++G(d,p) basis set. All other calculations were done using the B3LYP/6-311++G(d,p) geometries and ZPE corrections. [c] From ref 29. Binding energies are given for the most stable isomer of hydroxylammonium nitrate (HAN); geometries were optimized by the B3LYP/6-311++G(d,p) method.

in the B3LYP-DFT torsion potential, which otherwise is qualitatively similar to the MP2-optimized torsion potential.

To summarize, the UN molecule in the gas phase has the structure of an acid−base complex stabilized primarily by the hydrogen-bonding interactions due to partial donation of the acidic proton from HNO_3 to urea. In urea the electronegative O and N atoms can serve as the proton acceptor sites. Thus, two major isomers **7** and **8** can be formed as a result of the partial protonation of urea by HNO_3 at either the carbonyl or amino groups, respectively. Both isomers have the lowest energy conformations **7a** and **8a** that are distinctly more stable than other forms found as shallow local minima on the torsion potential energy profiles for the urea nitrate isomers. In fact, these other forms, e.g., **7b**, **7c**, and **8b**, are easily converted to the more favorable **a**-forms via torsional motions hindered by barriers of less than 0.1 kcal/mol.

Enthalpy of Formation of Gaseous Urea Nitrate. In the following discussion, for brevity we will omit letters from the isomer notations and collectively refer to forms **7a**−**c** and **8a,b** as isomers **7** and **8**, respectively. Their energetic and molecular parameters will be taken as those of the most stable **a**-conformations. It is worth noting that geometric parameters optimized in this study by the B3LYP-DFT and MP2 methods with the 6-311++G(d,p) basis set are very consistent with each other, and our optimized geometries of the most stable isomer **7** closely agree with those reported by Kohno et al.,[6] who used B3LYP-DFT and MP2 optimization methods with the 6-31++G-(2df,p) basis set. The structures optimized with the BB1K density functional have slightly shorter covalent bonds compared to those predicted by the B3LYP-DFT and MP2 methods; the differences are in the range of 0.01−0.04 Å. These differences are consistent with a relatively large fraction (42%) of HF exchange in the BB1K functional (the HF level of theory systematically underestimates covalent bond lengths). All optimization methods predict fairly consistent values for the lengths of hydrogen bonds in both **7** and **8**.

We can estimate the enthalpies of formation of the urea nitrate isomers in the gas phase on the basis of their calculated binding energies and experimental enthalpies of formation of urea[44] and nitric acid.[49] Table 1 lists the binding energies for molecular complexes **7** and **8** calculated as the enthalpies of the following reactions:

$$\mathbf{7} \rightarrow NH_2C(O)NH_2 + HNO_3 \quad (11)$$

$$\mathbf{8} \rightarrow NH_2C(O)NH_2 + HNO_3 \quad (12)$$

For comparison, we have also included in Table 1 the previously calculated binding energies of gaseous ammonium nitrate (AN)[27,29] and hydroxylammonium nitrate (HAN)[28,29] with respect to their dissociation according to eqs 13 and 14, respectively:

$$AN(g) \rightarrow NH_3 + HNO_3 \quad (13)$$

$$HAN(g) \rightarrow NH_2OH + HNO_3 \quad (14)$$

The basis set superposition error (BSSE) must be accounted for in order to derive more accurate interaction energies for molecular complexes. The BSSE results in unphysical lowering of the complex energy relative to the energies of separate fragments when finite basis sets are used to calculate the interaction energy. We applied the standard counterpoise (CP) correction,[50,51] which attempts to correct for energy lowering of each fragment by extending the basis set with ghost orbitals of the other fragment. Some reports, however, suggest that this scheme does not guarantee a systematic improvement of theoretical predictions.[52] Therefore, the binding energies of the hydrogen-bonded complexes of urea and ammonia with HNO_3 were evaluated with and without the counterpoise (CP) corrections; the extended 6-311+G(3df,2p) basis set was employed to get more accurate estimates. At all theory levels the CP corrections were applied a posteriori; i.e., they were calculated for structures optimized on the uncorrected potential energy surfaces. The results in Table 1 indicate that the magnitude of CP corrections strongly depends on the computational method and basis set. The smallest corrections (∼1 kcal/mol) are calculated for DFT methods with the 6-311++G(d,p) basis, and the largest CP values of 4−5 kcal/mol apply to MP2 and CCSD-(T) energies calculated with the 6-311G(d,p) basis set. The CP corrections decrease with increasing basis set, so that they amount to only 1−2 kcal/mol for MP2/6-311+G(3df,2p) and G2M methods. This warrants cautious optimism that the 6-311+G(3df,2p) basis set is sufficiently large to provide estimates of binding energies accurate to within 2 kcal/mol when used with correlated levels of theory, such as MP2 and G2M.

Different levels of theory consistently predict that urea nitrate isomer **7** is the strongest bound molecular complex, followed by the complexes of NH_2OH and NH_3 with HNO_3 and by isomer **8**. This in turn suggests that the urea O atom has a stronger base character than the N atoms in urea, NH_2OH, and NH_3. At the highest level of theory (G2M with CP correction) the binding energies for **7**, **8**, and AN(*g*) are 13.7, 8.3, and 10.2 kcal/mol, respectively. These binding energies in combination with the experimental enthalpies of formation ($\Delta_f H_0°$) of urea (−52.7 kcal/mol),[44] ammonia (−9.3 kcal/mol),[45] and nitric acid (−29.7 kcal/mol)[49] yield the following enthalpies of formation at $T =$ 0 K: $\Delta_f H_0°(\mathbf{7}) = \Delta_f H_0°(\mathbf{1}) + \Delta_f H_0°(HNO_3) - D_0°(\mathbf{7}) = -96.1$ kcal/mol, $\Delta_f H_0°(\mathbf{8}) = -90.7$ kcal/mol, and $D_f H_0°(AN) = -49.2$ kcal/mol. Including thermal corrections calculated using theoretical (B3LYP/6-311++G(d,p)) harmonic vibrational frequencies leads to the following values for the standard enthalpies of

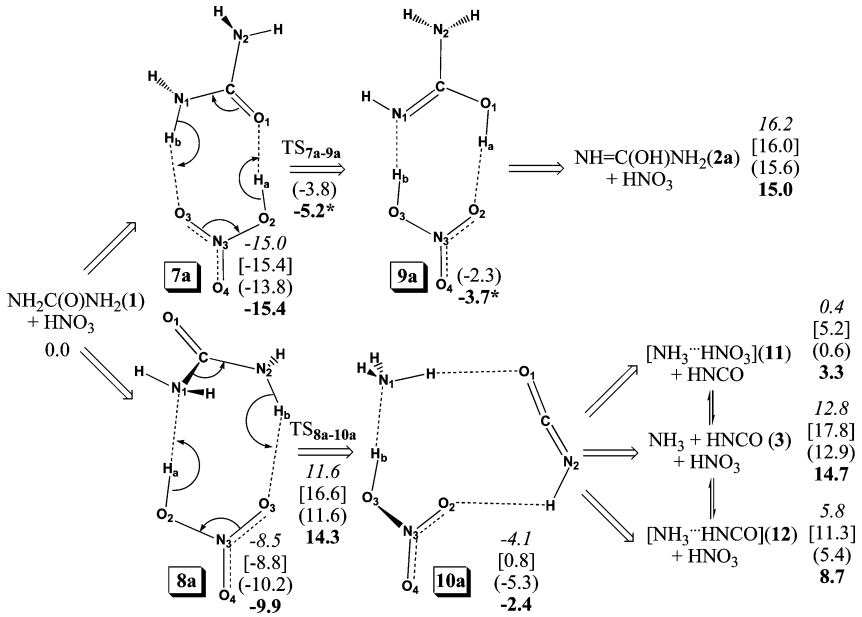

Figure 4. HNO_3-catalyzed urea transformations: eight-center pathways. All energies ($T = 0$ K, ZPE-corrected, in kcal/mol) are given relative to the reactants (urea + HNO_3) as calculated by the B3LYP-DFT (values in italics), BB1K-DFT (values in square brackets), and MP2 (values in parentheses) methods with the 6-311++G(d,p) basis set. The best values (in bold) were obtained at the G2M level. The G2M energies identified with an asterisk were calculated using the MP2/6-311++G(d,p) optimized geometries and ZPE corrections for those structures, which could not be optimized at the B3LYP/6-311++G(d,p) level.

formation of gaseous urea and ammonia nitrates: $\Delta_f H_{298}°$(**7**) = −102.3 kcal/mol, $\Delta_f H_{298}°$(**8**) = −97.1 kcal/mol, and $\Delta_f H_{298}°$(AN) = −53.8 kcal/mol. These estimates should be accurate to ±3 kcal/mol.

Regarding the performance of other methods listed in Table 1, we can comment that using a large basis set in combination with the second-order perturbation treatment of electron correlation is sufficient to obtain reliable binding energies for the molecular complexes studied. B3LYP and BB1K DFT functionals give very similar predictions of binding energies that are within 2 kcal/mol from the G2M benchmark values. However, the errors exhibit a nonsystematic behavior. For instance, DFT methods overestimate the stability of the ammonia−nitric acid complex and UN isomer **7** but underestimate the binding energy of isomer **8**.

Catalytic Effect of HNO_3 on Urea Transformations. Molecular complexes **7** and **8** are each stabilized by two hydrogen bonds between the urea and HNO_3 parts arranged in such a manner that makes possible a double proton transfer within the cyclic hydrogen-bonded structure. Figure 4 illustrates the mechanism of the double proton transfer in the most stable **a**-forms of complexes **7** and **8**, where two endocyclic protons may shift along the hydrogen bonds within the eight-membered rings. The double H-shift in **7** mediates the prototropic tautomerization of urea (a (1,3) H-shift between the N and O atoms), whereas the double proton transfer in **8** facilitates a (1,3) H-shift between the two N atoms which leads to the breakdown of the urea part to the HNCO and NH_3 fragments. In both cases, the HNO_3 part of either **7** or **8** is left chemically unchanged by the double proton transfer, so that HNO_3 effectively plays a catalytic role for the (1,3) H-shifts in urea by acting as a donor of the first, $H_{(a)}$, and an acceptor of the second, $H_{(b)}$, protons transferred in a relay fashion.

These catalytic reactions are rather peculiar from a mechanistic standpoint because they involve several bond-breaking and -forming processes for which either a stepwise or a concerted mechanism could be envisaged. A stepwise mechanism could be initiated by a hypothetical transfer of the single acidic $H_{(a)}$ proton from HNO_3 to urea in either **7** or **8**, yielding ion pairs composed of the nitrate and protonated urea ions. Then another proton ($H_{(b)}$) would have to be transferred back to the nitrate ion. These two sequential H-shifts would transform the urea part of **7** to its enolic form, whereas the urea part in **8** would become a zwitterion

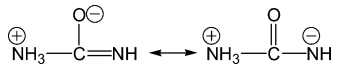

which could further undergo the C−N bond fission to produce NH_3 and HNCO. On the other hand, a concerted mechanism implies that all bond-breaking and -forming processes must occur simultaneously, without any ionic intermediates. As follows from Figure 4, our calculations indicate that the double proton transfers in both **7a** and **8a** occur in one step, via $TS_{\mathbf{7a-9a}}$ and $TS_{\mathbf{8a-10a}}$, respectively. To get more detailed mechanistic insights, we optimized and examined the intrinsic reaction pathways[26] passing through $TS_{\mathbf{7a-9a}}$ and $TS_{\mathbf{8a-10a}}$. For example, Figure 5 illustrates the geometric changes along the reaction path for the HNO_3-catalyzed urea decomposition via the 8-center $TS_{\mathbf{8a-10a}}$. We have followed the intrinsic reaction coordinate from $TS_{\mathbf{8a-10a}}$ far into the forward and reverse directions. The reaction pathways calculated at the MP2 and B3LYP-DFT levels of theory with the 6-311++G(d,p) basis set have very similar features. For clarity, only MP2 results are given in Figure 5.

The left-hand side of the reaction profile features two shoulders associated with the double proton transfer on the way from complex **8a** to $TS_{\mathbf{8a-10a}}$. In the early stages, the reaction involves mainly the motion of the acidic proton $H_{(a)}$ from the $O_{(2)}$ atom of HNO_3 to the $N_{(1)}$ atom of urea (here we use the atomic numbering scheme shown in Figure 4). After the first proton transfer is essentially complete, molecular structures along the reaction pathway have a strong ionic character. However, the electrostatic interactions in the ion pair of [$NH_3C(O)NH_2^+$] and [NO_3^-] are not strong enough to stabilize the ionic form urea nitrate in the gas phase, so it appears as a shoulder rather than an intermediate on the reaction profile.

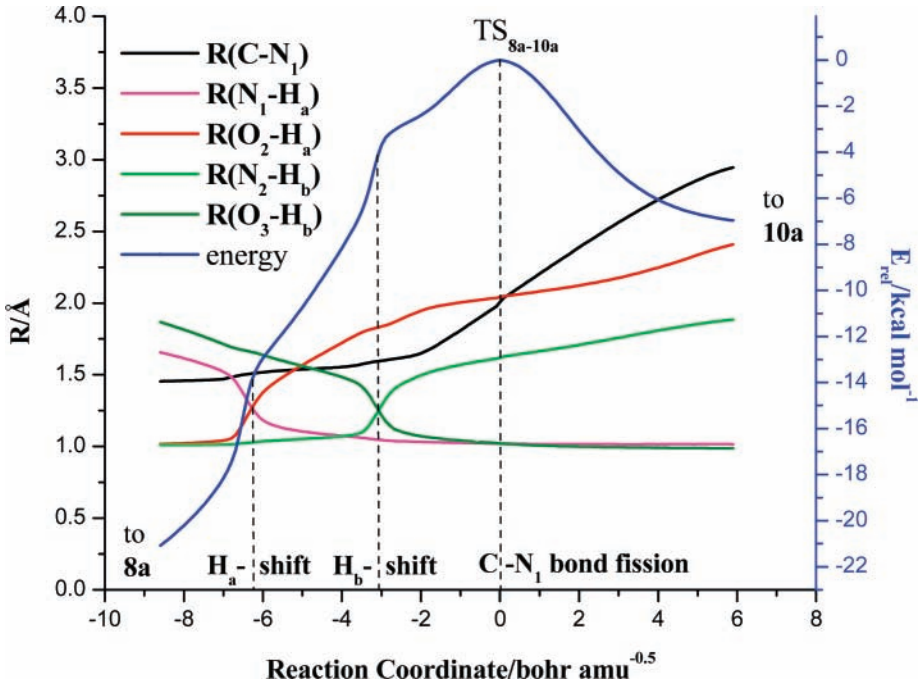

Figure 5. Energetic profile ($T = 0$ K, without ZPE correction) and changes in selected bond lengths along the IRC path for the TS_{8a-10a} calculated at the MP2/6-311++G(d,p) level of theory with a step size of 0.05 bohr/amu$^{0.5}$.

Meanwhile, the reaction pathway ascends further as the reaction coordinate becomes dominated by the motion of the second proton $H_{(b)}$ from the $N_{(2)}$ atom of urea to the $O_{(3)}$ atom of HNO_3. The second shoulder on the reaction profile signifies the completion of the second proton transfer. The transient structures immediately after the double proton transfer in **8a** are reminiscent of the urea zwitterion associated with HNO_3. Again, this zwitterionic structure is unstable in the gas phase, so it appears only as a shoulder on the reaction profile.

The reaction profile shown in Figure 5 reaches TS_{8a-10a} only in the final stages when the reaction coordinate is clearly dominated by the breaking of the $C-N_{(1)}$ bond, which has been weakly coupled to the first and second proton transfers in the earlier stages. The $C-N_{(1)}$ bond-breaking yields the NH_3, HNCO, and HNO_3 molecules bound together in a termolecular complex **10**. The geometry optimization starting from the points on the right-hand side of the IRC profile ultimately leads to conformation **10a** (Figure 4), where the HNCO part can be viewed as attached to the ammonium nitrate molecular complex. This is the most stable form of complex **10** found in this study, with a G2M binding energy of 17.1 kcal/mol relative to the $NH_3 + HNO_3 + HNCO$. Although several other (less stable) conformations of **10** have also been found, we did not pursue their explicit characterization. Performing a detailed conformational analysis for **10** would be a very difficult task given the flexibility of this termolecular complex with respect to the internal rotations of its parts, which result in a large number of plausible conformations and pathways between them. The common structural feature of various forms of complex **10** is the presence of three components ($HNCO + NH_3 + HNO_3$) with different mutual orientation. These components and their bimolecular complexes (e.g., ammonium nitrate and isocyanate) are expected to be the ultimate products of the urea nitrate decomposition via TS_{8a-10a}.

Figure 5 reveals that the double proton transfer in **8a** proceeds in a relay fashion, which combines the elements of both stepwise and concerted mechanisms. This reaction is concerted in a sense that it proceeds in a single step, without any ionic intermediates. However, the reaction coordinate undergoes substantial changes on the way from the reactant to the products, almost as if the mechanism was stepwise. Furthermore, the mechanism of this reaction will probably become truly stepwise in the condensed phases (e.g., in solution), where ionic intermediates discussed above exist as local minima.

For the HNO_3-catalyzed urea tautomerization channel (**1** + $HNO_3 \rightarrow$ **7a** $\rightarrow TS_{7a-9a} \rightarrow$ **9a** $\rightarrow$ **2a** + HNO_3), we should note that the local minimum **9a** (the complex of HNO_3 with the enolic form of urea) and TS_{7a-9a} could be found on the MP2/6-311++G(d,p) PES; however, these stationary points are completely washed out on the B3LYP-DFT PES. In fact, even at the MP2 level of theory the energy of TS_{7a-9a} falls below the energy level of complex **9a** after inclusion of the zero-point vibrational energy corrections. Hence, the HNO_3-catalyzed eight-center urea tautomerization pathway can be simply written as a two-step sequence: **1** + $HNO_3 \rightarrow$ **7a** $\rightarrow$ **2a** + HNO_3. Neither the first nor the second steps have a well-defined transition state. Thus, the conversion of $H_2NC(O)NH_2$ (**1**) to $H_2NC(OH)NH$ (**2a**) in the presence of HNO_3 is controlled solely by the reaction endothermicity of 15.0 kcal/mol. The reverse reaction assisted by HNO_3 is predicted to proceed without any barrier. Under such circumstances, the enolic forms of urea (**2a**−**2d**) are not expected to accumulate in any significant quantities. In principle, they may further decompose by either NH_3 or H_2O elimination channels (see Figure 1), but the corresponding reaction barriers are so high that $H_2NC(OH)NH$ is more likely to isomerize back to urea rather than follow the unimolecular decomposition pathways.

Besides the eight-center pathways shown in Figure 4, the HNO_3-catalyzed transformations of urea can be accomplished via the six-center pathways originating from the urea nitrate conformations **7b**/**7c** and **8b**. These pathways are presented in Figure 6. They are fairly similar to the eight-center pathways in a sense that they also involve concerted double proton transfers, but here the same $O_{(2)}$ atom of nitric acid acts as the proton donor and acceptor, and the protons are relayed within the six-center hydrogen-bonding structures. These reactions involve six-center transition states TS_{7b-9b} and TS_{8b-10b} well-defined at both the MP2 and B3LYP-DFT levels of theory. The

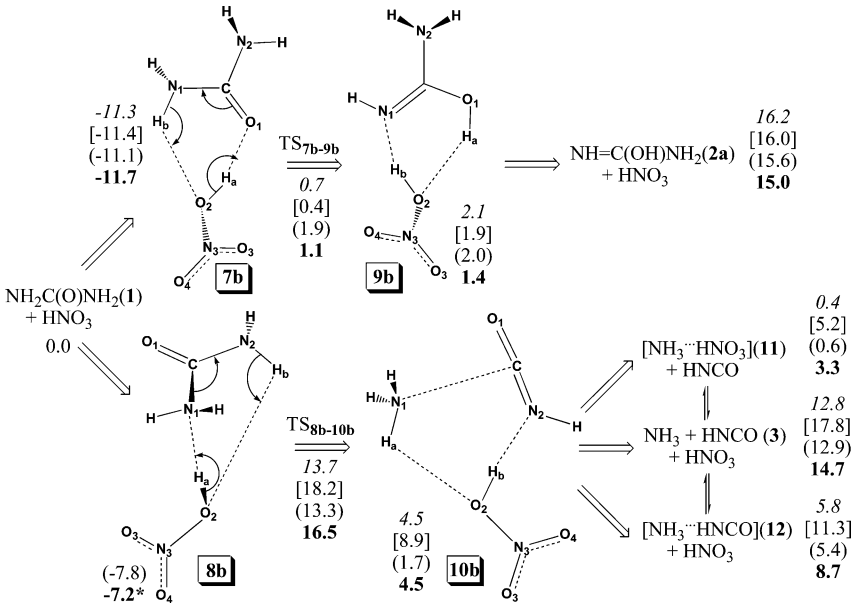

Figure 6. HNO_3-catalyzed urea transformations: six-center pathways. All energies ($T = 0$ K, ZPE-corrected, in kcal/mol) are given relative to the reactants (urea + HNO_3) as calculated by the B3LYP-DFT (values in italics), BB1K-DFT (values in square brackets), and MP2 (values in parentheses) methods with the 6-311++G(d,p) basis set. The best values (in bold) are obtained at the G2M level. The G2M energies identified with an asterisk are calculated using the MP2/6-311++G(d,p) optimized geometries and ZPE corrections for those structures, which could not be optimized at the B3LYP/6-311++G(d,p) level.

energies of TS_{7b-9b} and TS_{8b-10b} are slightly higher than those of the eight-center TS_{7a-9a} and TS_{8a-10a}. Nevertheless, the energy of TS_{7b-9b} falls below the energy level of **9b** after inclusion of the zero-point vibrational energy corrections, as was the case for TS_{7a-9a} and **9a**. Thus, the HNO_3-catalyzed conversion of $H_2NC(OH)NH$ to $H_2NC(O)NH_2$ effectively proceeds without a barrier via both the six- and eight-center reaction pathways. The effective G2M barrier for the urea decomposition to HNCO and NH_3 assisted by HNO_3 via the six-center pathway is 16.5 kcal/mol, which is ~2 kcal/mol higher than the barrier for the analogous eight-center decomposition pathway via TS_{8a-10a}. This difference is fairly small, so that both six- and eight-center decomposition pathways are expected to be competitive. The IRC calculation for the six-center TS_{8b-10b} in forward direction connects it to the termolecular complex **10b**, which is stabilized by 10.2 kcal/mol with respect to the separated fragments (NH_3 + HNCO + HNO_3). The latter fragments as well as their bimolecular complexes (e.g., ammonium nitrate and isocyanate) are expected to be the ultimate products of the urea nitrate decomposition via both the six- and eight-center decomposition pathways.

Nucleophilic Reactions of HNO_3 with Urea. In the reactions of urea with HNO_3 considered above, HNO_3 effectively plays a role of a dual acid−base catalyst for urea isomerization and decomposition. Besides acting as a proton donor, HNO_3 may also attack the carbonyl C atom of urea as a nucleophile. Figure 7 illustrates the mechanisms of two nucleophilic reactions of HNO_3 with urea concerted with proton transfers from HNO_3 to either O or N atoms of urea.

The first pathway originates from the molecular complex **7a** and involves a proton transfer from HNO_3 to the urea O atom coupled with a nucleophilic attack of the $O_{(3)}$ nitrate oxygen atom on the urea C atom. This pathway leads to the addition of HNO_3 to the carbonyl group producing intermediate **13** with a tetrahedral carbon center. This intermediate easily rearranges back to **7a** over a barrier of ~3 kcal/mol, according to the MP2/6-311++G(d,p) and G2M energetics based on the MP2-optimized structure of **13**. The latter barrier is reduced to 1.8 kcal/mol at the BB1K/6-311++G(d,p) level, whereas the

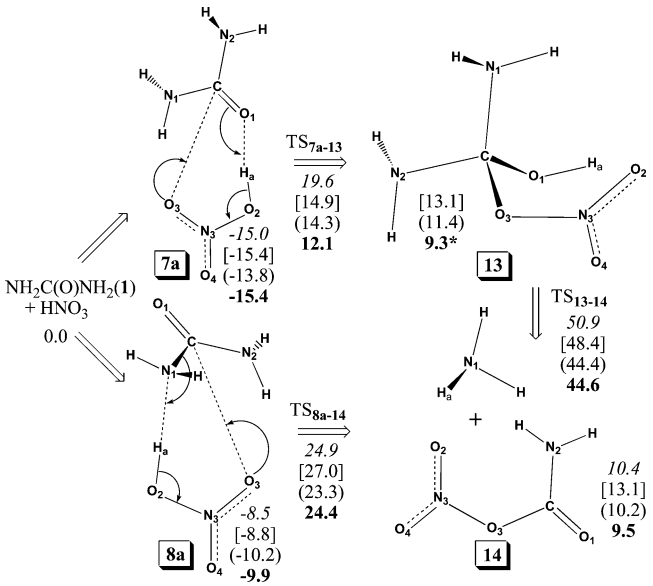

Figure 7. Nucleophilic reactions of HNO_3 with urea. All energies ($T = 0$ K, ZPE-corrected, in kcal/mol) are given relative to the reactants (urea + HNO_3) as calculated by the B3LYP-DFT (values in italics), BB1K-DFT (values in square brackets), and MP2 (values in parentheses) methods with the 6-311++G(d,p) basis set. The best values (in bold) were obtained at the G2M level. The G2M energies identified with an asterisk were calculated using the MP2/6-311++G(d,p) optimized geometries and ZPE corrections for those structures, which could not be optimized at the B3LYP/6-311++G(d,p) level.

B3LYP/6-311++G(d,p) method fails to find a local minimum corresponding to intermediate **13**. Its alternative transformations, such as H_2O or NH_3 eliminations, are not likely to be competitive. For example, the NH_3 elimination producing an anhydride of nitric and carbamic acids (**14**) has a barrier of >30 kcal/mol (see Figure 7).

In the second pathway originating from the molecular complex **8a**, the nucleophilic attack of $O_{(3)}$ nitrate oxygen atom on the urea C atom is concerted with the proton transfer from HNO_3 to the N atom in urea (see Figure 7). The protonation of

SCHEME 4

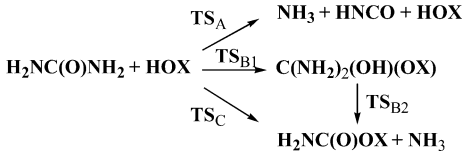

TABLE 2: Summary of Energetic Parameters[a] for Reactions of Urea with H_2O and HNO_3

	X = H[b]		X = NO_2[c]
species	CBS-QB3	B3LYP/6-31G**	G2M
$H_2NC(O)NH_2$ + XOH	0.0	0.0	0.0
TS_A	24.9	16.7	14.3
NH_3 + HNCO +XOH	15.2	16.5	14.7
TS_{B1}	47.0	41.6	12.1
$C(NH_2)_2(OH)(OX)$	13.5	13.7	9.3
TS_{B2}		41.9	44.6
TS_C	47.9	41.3	24.4
$H_2NC(O)OX$ + NH_3	−1.2	−4.6	9.5

[a] Relative energies (ZPE-corrected, in kcal/mol, $T = 0$ K) are given with respect to the reactants (urea + XOH). [b] From ref 9. [c] This work.

urea at the N atom releases a neutral NH_3 molecule, while the ONO_2 anion takes its place at the C atom. This pathway effectively results in the direct nucleophilic substitution at the C atom in **8a**, producing anhydride **14** over a barrier of 24.4 kcal/mol (G2M) with respect to the energy level of urea and HNO_3. The latter barrier is about 10 kcal/mol higher than that for the HNO_3-catalyzed urea decomposition to HNCO + NH_3 (see Figure 4). Therefore, anhydride **14** may be produced only as a minor coproduct during the gas-phase decomposition of urea nitrate. At high temperature, **14** should readily decompose to CO_2 + N_2O + H_2O.

Similarities of the Reactions of Urea with H_2O and HNO_3. It is instructive to compare our results for the reaction of urea with HNO_3 with those for the hydrolysis of urea reported recently by Tsipis and Karipidis.[9] The two reactions proceed via similar channels, which can be summarized in a single mechanism shown in Scheme 4. Channel A corresponds to the HOX-catalyzed (X = H, NO_2) urea decomposition to NH_3 and HNCO. Channel B is a two-step addition−elimination sequence: (i) HOX addition to the carbonyl group forming an intermediate with a tetrahedral carbon center; (ii) NH_3 elimination from this intermediate. Channel C is a concerted S_N-type nucleophilic substitution at the urea C atom. The transition states TS_A, TS_{B1}, TS_{B2}, and TS_C correspond to TS_{28-29}, TS_{10-11}, TS_{9-10}, and TS_{7-12} for X = H reported by Tsipis and Karipidis[9] and to TS_{8a-10a}, TS_{7a-13}, TS_{13-14}, and TS_{8a-14} for X = NO_2 (see Figures 4 and 7). For simplicity, molecular complexes formed by the reactants and products are omitted from Scheme 4.

The reliable energies for the urea + HOX reactions have been calculated at the high levels of theory: CBS-QB3 for X = H (from Tsipis and Karipidis[9]) and G2M for X = NO_2 (this work). Their comparison (see Table 2) reveals that all three initial reactions of urea with HNO_3 have lower barriers than those with H_2O, which is reasonable taking into account the stronger acidity of HNO_3 and the less strained structure of TS_A, TS_{B1}, and TS_C for the reactions of urea with HNO_3 vs those involved in the urea hydrolysis. On the other hand, the barrier for NH_3 elimination from $C(NH_2)_2(OH)(OX)$ is fairly high in both cases. As a result, the concerted substitution (channel C) is more favorable than the stepwise channel B for the reaction with HNO_3, whereas these two channels have comparable barriers for the reaction with H_2O. However, the most favorable channel in both cases is the HOX-catalyzed urea breakdown (channel A). Similar processes to those summarized in Scheme 4 are expected to be involved in the reactions of urea with other HOX species, such as alcohols, organic and mineral acids, etc.

IV. Summary of Reaction Pathways and Conclusions

Gas-phase urea nitrate is an acid−base complex stabilized primarily by partial proton transfer from HNO_3 to urea. Two isomers, **7** and **8**, are formed by hydrogen bonding of the acidic proton of HNO_3 with the carbonyl or amino groups of urea, respectively. Figure 8 summarizes various reaction pathways from **7** and **8** computed at the G2M level of theory (only transformations of the lowest energy conformations are shown). For comparison, we have also shown the decomposition pathway **7** → TS1 → INT1 → TS2 → HNCO + NH_3 + HNO_3 computed by Kohno et al.[6] at the MP2/6-31++G(2d,p) level of theory.

Molecular complexes **7** and **8** can undergo relatively facile double proton transfers within cyclic hydrogen-bonded networks (see Figure 8). The double H-shift in **7** mediates the keto−enol tautomerization of urea via TS_{7-9}, whereas the double H-transfer in **8** facilitates the breakdown of the urea part to the HNCO and NH_3 via TS_{8-10}. In these reactions, HNO_3 plays a catalytic

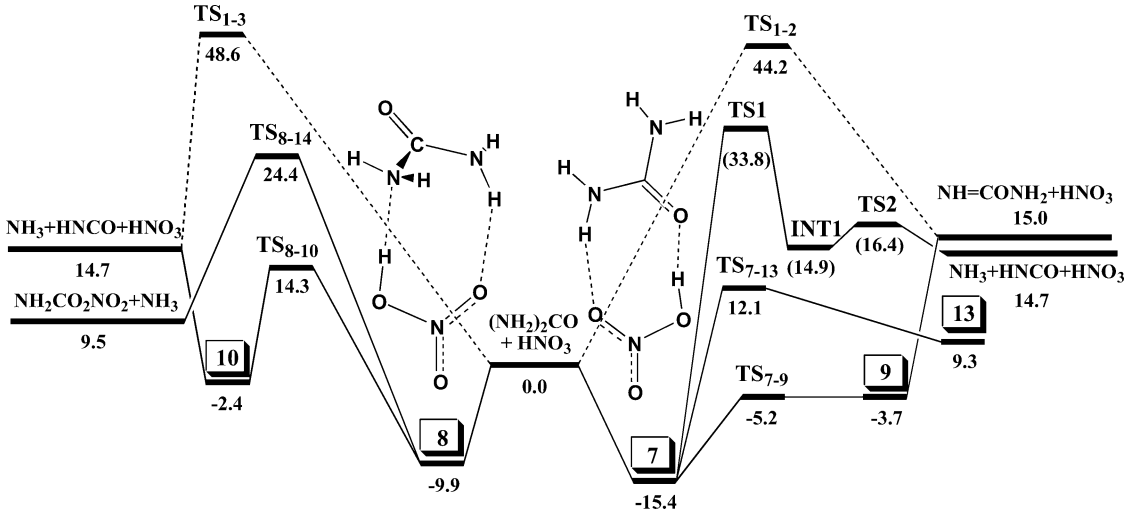

Figure 8. Schematic potential energy diagram of the urea nitrate decomposition pathways in the gas phase. Energies ($T = 0$ K, ZPE-corrected, in kcal/mol) are given relative to urea + HNO_3 as calculated in this work by the G2M method. The values in parentheses were calculated at the MP2/6-31++G(2d,p) level by Kohno et al.[6]

role for the (1,3) H-shifts in urea by acting as a donor of the first and an acceptor of the second protons transferred in a relay fashion, which combines elements of both stepwise and concerted mechanisms. The HNO_3-catalyzed pathways of urea tautomerization and decomposition have substantially lower effective barriers than the analogous uncatalyzed reactions, which require (1,3) H-shifts via more strained four-center transition states TS_{1-2} and TS_{1-3}. In particular, the conversion of urea to its enolic form in the presence of HNO_3 is controlled solely by the reaction endothermicity of 15.0 kcal/mol. However, the enolic form is not expected to accumulate in significant quantities in the presence of HNO_3 due to its very facile conversion back to urea, which is barrierless when assisted by HNO_3. Our predicted HNO_3-catalyzed pathway for urea breakdown to HNCO and NH_3 has an effective barrier of 14.3 kcal/mol (TS_{8-10}), which is much lower than the barrier involved in the previously proposed[6] decomposition pathway via **7**, TS1, INT1, and TS2 (see Figure 8), where HNO_3 does not directly participate in the rate-controlling (1,3) H-transfer step (see Scheme 1).

Molecular complexes **7** and **8** may also undergo single proton transfer from HNO_3 to urea coupled with a nucleophilic attack of the nitrate oxygen atom on the urea C atom. These pathways lead from **7** to the relatively unstable intermediate **13**, which easily rearranges back to **7**, and from **8** to the anhydride of nitric and carbamic acids (**14**). However, the barrier involved in the latter process is 10 kcal/mol higher than that for the HNO_3-catalyzed urea decomposition. Thus, HNCO + NH_3 + HNO_3 and their association products (i.e., ammonium nitrate and isocyanate) are expected to be the major initial products of the urea nitrate decomposition in the gas phase. This prediction is consistent with the experimental *T*-jump/FTIR observations.[5] The H_2O, CO_2, and N_2O products observed at higher temperatures can be formed from the secondary reactions of HNCO and HNO_3 initiated by the homolytic dissociation of HNO_3 to OH + NO_2. The same H_2O, CO_2, and N_2O products can be expected for the decomposition of anhydride **14**, but the pathways involving **14** probably play a minor role in the mechanism of the urea nitrate decomposition.

Acknowledgment. This work was supported by a DOD MURI grant managed by the Army Research Office and by the Air Force Office of Scientific Research.

Supporting Information Available: Tables S1−S3 containing the geometries for all species and transition states calculated in this study; Tables S4−S7 listing energies calculated at various theoretical levels. This material is available free of charge via the Internet at http://pubs.acs.org.

References and Notes

(1) Sandstrom, F. W.; Abernathy, R. L.; Leone, M. G.; Banks, M. L. *AIP Conf. Proc.* **1999**, *505*, 825−828.

(2) Hiyoshi, R. I.; Nakamura, J. *Proc. Int. Symp. Anal. Det. Expl.* **1998**, *6th*, 15.

(3) Hiyoshi, R. I.; Nakamura, J. *Kayaku Gakkaishi* **2000**, *61*, 120.

(4) Howard, W. M.; Fried, L. E.; Souers, P. C.; Vitello, P. A. *AIP Conf. Proc.* **2002**, *620*, 161−164.

(5) Hiyoshi, R. I.; Brill, T. B.; Kohno, Y.; Takahashi, O.; Saito, K. *12th Int. Detonation Symp.*, Aug 11−16, San Diego, CA, 2002.

(6) Kohno, Y.; Takahashi, O.; Hiyoshi, R. I.; Nakamura, J.; Saito, K. *J. Phys. Chem. A* **2003**, *107*, 6444.

(7) Wöhler, F. *Poggendorff's Ann. Phys.* **1828**, *12*, 253−256.

(8) Tsipis, C. A.; Karipidis, P. A. *J. Am. Chem. Soc.* **2003**, *125*, 2307−2318.

(9) Tsipis, C. A.; Karipidis, P. A. *J. Phys. Chem. A* **2005**, *109*, 8560−8567.

(10) Estiu, G.; Merz, K. M., Jr. *J. Am. Chem. Soc.* **2004**, *126*, 6932−6944.

(11) Frisch, M. J.; Trucks, G. W.; Schlegel, H. B.; Scuseria, G. E.; Robb, M. A.; Cheeseman, J. R.; Montgomery, J. A., Jr.; Vreven, T.; Kudin, K. N.; Burant, J. C.; Millam, J. M.; Iyengar, S. S.; Tomasi, J.; Barone, V.; Mennucci, B.; Cossi, M.; Scalmani, G.; Rega, N.; Petersson, G. A.; Nakatsuji, H.; Hada, M.; Ehara, M.; Toyota, K.; Fukuda, R.; Hasegawa, J.; Ishida, M.; Nakajima, T.; Honda, Y.; Kitao, O.; Nakai, H.; Klene, M.; Li, X.; Knox, J. E.; Hratchian, H. P.; Cross, J. B.; Bakken, V.; Adamo, C.; Jaramillo, J.; Gomperts, R.; Stratmann, R. E.; Yazyev, O.; Austin, A. J.; Cammi, R.; Pomelli, C.; Ochterski, J. W.; Ayala, P. Y.; Morokuma, K.; Voth, G. A.; Salvador, P.; Dannenberg, J. J.; Zakrzewski, V. G.; Dapprich, S.; Daniels, A. D.; Strain, M. C.; Farkas, O.; Malick, D. K.; Rabuck, A. D.; Raghavachari, K.; Foresman, J. B.; Ortiz, J. V.; Cui, Q.; Baboul, A. G.; Clifford, S.; Cioslowski, J.; Stefanov, B. B.; Liu, G.; Liashenko, A.; Piskorz, P.; Komaromi, I.; Martin, R. L.; Fox, D. J.; Keith, T.; Al-Laham, M. A.; Peng, C. Y.; Nanayakkara, A.; Challacombe, M.; Gill, P. M. W.; Johnson, B.; Chen, W.; Wong, M. W.; Gonzalez, C.; Pople, J. A. *Gaussian 03*, revision B.04; Gaussian, Inc.: Wallingford, CT, 2004.

(12) Parr, R. G.; Yang, W. *Density Functional Theory of Atoms and Molecules*; Oxford University Press: New York, 1989.

(13) Koch, W.; Holthausen, M. C. *A Chemist's View of Density Functional Theory*; Wiley-VCH: Weinheim, 2000.

(14) (a) Becke, A. D. *J. Chem. Phys.* **1993**, *98*, 5648. (b) Becke, A. D. *Phys. Rev. A* **1988**, *38*, 3098. (c) Lee, C.; Yang, W.; Parr, R. G. *Phys. Rev. B* **1988**, *37*, 785. (d) Stephens, P. J.; Devlin, F. J.; Chabalowski, C. F.; Frisch, M. J. *J. Phys. Chem.* **1994**, *98*, 11623.

(15) Zhao, Y.; Lynch, B. J.; Truhlar, D. G. *J. Phys. Chem. A* **2004**, *108*, 2715. BB1K can be called in GAUSSIAN 03 by the following keywords in the route section: bb95 IOp(3/76=0580004200). Additional information on the implementation of BB1K can be found on the Internet at http://comp.chem.umn.edu/info/bb1k.htm.

(16) Becke, A. D. *J. Chem. Phys.* **1996**, *104*, 1040−1046.

(17) The performance of the B3LYP functional for geometry optimization was assessed, for example, by the authors of the G2M (ref 30), G3//B3LYP (Baboul, A. G.; Curtiss, L. A.; Redfern, P. C.; Raghavachari, K. *J. Chem. Phys.* **1999**, *110*, 7650), and G3X (Curtiss, L. A.; Redfern, P. C.; Raghavachari, K.; Pople, J. A. *J. Chem. Phys.* **2001**, *114*, 108) model chemistries.

(18) Zhao, Y.; Gonzales-Garcia, N.; Truhlar, D. G. *J. Phys. Chem. A* **2005**, *109*, 2012−2018.

(19) Zhao, Y.; Truhlar, D. G.. *J. Phys. Chem. A* **2005**, *109*, 5656−5667.

(20) Pople, J. A.; Head-Gordon, M.; Raghavachari, K. *J. Chem. Phys.* **1987**, *87*, 5968.

(21) Sadhukhan, S.; Munoz, D.; Adamo, C.; Scuseria, G. E. *Chem. Phys. Lett.* **1999**, *306*, 83.

(22) Pavese, M.; Chawla, S.; Lu, D.; Lobaugh, J.; Voth, G. A. *J. Chem. Phys.* **1997**, *107*, 7428.

(23) Meuwly, M.; Bach, A.; Leutwyler, S. *J. Am. Chem. Soc.* **2001**, *123*, 11446.

(24) Peng, C.; Ayala, P. Y.; Schlegel, H. B.; Frisch, M. J. *J. Comput. Chem.* **1996**, *17*, 49.

(25) (a) Csaszar, P.; Pulay, P. *J. Mol. Struct. (THEOCHEM)* **1984**, *114*, 31. (b) Farkas, O.; Schlegel, H. B. *J. Chem. Phys.* **1999**, *111*, 10806.

(26) (a) Gonzalez, C.; Schlegel, H. B. *J. Chem. Phys.* **1989**, *90*, 2154−2161. (b) Gonzalez, C.; Schlegel, H. B. *J. Phys. Chem.* **1990**, *94*, 5523−5527.

(27) Alavi, S.; Thompson, D. L. *J. Chem. Phys.* **2002**, *117*, 2599−2608.

(28) Alavi, S.; Thompson, D. L. *J. Chem. Phys.* **2003**, *119*, 4274−4282.

(29) Alavi, S.; Thompson, D. L. *J. Phys. Chem. A* **2004**, *108*, 8801−8809.

(30) Mebel, A. M.; Morokuma, K.; Lin, M. C. *J. Chem. Phys.* **1995**, *103*, 7414.

(31) Pople, J. A.; Krishnan, R.; Schlegel, H. B.; Binkley, J. S. *Int. J. Quantum Chem.* **1978**, *14*, 545.

(32) Pople, J. A.; Head-Gordon, M.; Raghavachari, K. *J. Chem. Phys.* **1987**, *87*, 7382.

(33) Watts, J. D.; Gauss, J.; Bartlett, R. J. *J. Chem. Phys.* **1993**, *98*, 8718.

(34) Hampel, C.; Peterson, K.; Werner, H.-J. *Chem. Phys. Lett.* **1992**, *190*, 1.

(35) Levine, I. N. *Quantum Chemistry*; Prentice Hall: Englewood Cliffs, NJ, 1991.

(36) Meier, R. J.; Coussens, B. *J. Mol. Struct. (THEOCHEM)* **1992**, *253*, 25.

(37) Ramondo, F.; Bencivenni, L.; Rossi, V.; Caminiti, R. *J. Mol. Struct. (THEOCHEM)* **1992**, *277*, 185.

(38) Kontoyianni, M.; Bowen, J. P. *J. Comput. Chem.* **1992**, *13*, 657.

(39) Dixon, D. A.; Matsuzawa, N. *J. Phys. Chem.* **1994**, *98*, 3967.

(40) Godfrey, P. D.; Brown, R. R.; Hunter, A. N. *J. Mol. Struct.* **1997**, *413*, 405.

(41) Spoliti, M.; Pieretti, A.; Bencivenni, L.; Sanna, N. *Electron. J. Theor. Chem.* **1997**, *2*, 149.

(42) Masunov, A.; Dannenberg, J. J. *J. Phys. Chem. A* **1999**, *103*, 178.
(43) Gobbi, A.; Frenking, G. *J. Am. Chem. Soc.* **1993**, *115*, 2362.
(44) Frenkel, M.; Marsh, K. N.; Wilhoit, R. C.; Kabo, G. J.; Roganov, G. N. *Thermodynamics of Organic Compounds in the Gas State*; Thermodynamics Research Center: College Station, TX, 1994.
(45) Cox, J. D.; Wagman, D. D.; Medvedev, V. A. *CODATA Key Values for Thermodynamics*; Hemisphere: New York, 1989.
(46) Schuurman, M. S.; Muir, S. R.; Allen, W. D.; Schaefer, H. F., III *J. Chem. Phys.* **2004**, *120*, 11586.
(47) Worsham, J. E.; Busing, W. R. *Acta Crystallogr.* **1969**, *B25*, 572.
(48) Harkema, S.; Feil, D. *Acta Crystallogr.* **1969**, *B25*, 589.
(49) Gurvich, L. V.; Veyts, I. V.; Alcock, C. B. *Thermodynamic Properties of Individual Substances*, 4th ed.; Hemisphere: New York, 1989.
(50) Jansen, H. B.; Ross, P. *Chem. Phys. Lett.* **1969**, *3*, 140.
(51) Boys, S. F.; Bernardi, F. *Mol. Phys.* **1970**, *19*, 553.
(52) (a) Schwenke, D. W.; Truhlar, D. G. *J. Chem. Phys.* **1984**, *82*, 2418. (b) Frisch, M. J.; Del Bene, J. E.; Binkley, J. S.; Schaefer, H. F., III. *J. Chem. Phys.* **1986**, *84*, 2279. (c) Cook, D. B.; Sordo, J. A.; Sordo, T. L. *Int. J. Quantum Chem.* **1993.** *48*, 375.